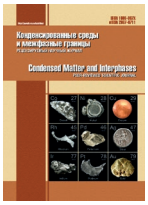

ISSN 1606-867X (Print)
ISSN 2687-0711 (Online)
Condensed Matter and Interphases
Kondensirovannye Sredy i Mezhfaznye Granitsy
https://journals.vsu.ru/kcmf/

Original articles

Research article
https://doi.org/10.17308/kcmf.2022.24/10551

Computer model of Cu-Ni-Mn isobaric phase diagram: verification of crystallisation intervals and change of the three-phase reaction type

A. E. Zelenaya✉, V. I. Lutsyk, V. D. Baldanov

Institute of Physical Materials Science, Siberian Branch of the Russian Academy of Sciences,
8 Sakhyanovoy str., Ulan-Ude 670047, Russian Federation

Abstract

The purpose of article was to show the possibilities of spatial computer models of phase diagrams in solving of the problems of digitalization of materials science. The study of the high-temperature part of the isobaric phase diagram for the Cu–Ni–Mn system was carried out taking into account two polymorphic modifications of manganese (δMn and γMn). For a better understanding of the phase diagram structure, at the first stage, its prototype was developed with increased temperature and concentration intervals between binary points with the preservation of topological structure, which is then modified into the model of phase diagram corresponding to the real system. The phase diagram of Cu-Mn-Ni system above 800°C was formed by three pairs of liquidus, solidus, and transus surfaces and three ruled surfaces with a horizontal arrangement of the forming segment.

Experimental part: the effect of changing the peritectic equilibrium (L + δMn → γMn) to the metatectic one (δMn → L + γMn) was revealed. The crystallisation features at the change of three-phase transformation type were considered, the surface of change of melt mass increment sign and the vertical mass balances for the three-phase region L + δMn + γMn were constructed. The surface of two-phase reaction, on which the change of three-phase reaction type occurs, is a ruled surface and is determined, using the algorithm for calculating the change in sign of the mass increment of liquid phase. Three-phase region, taking into account the surface of type change of three-phase reaction, is divided into six concentration fields when projecting into the triangle of compositions. Four concentration fields differ in the crystallisation stages and the formed set of microstructures. Isothermal sections were calculated in the temperature range between two minimum points arranged in the Cu–Mn and Mn–Ni systems at zero crystallisation interval between the valleys of the liquidus and solidus surfaces and taking into account the crystallisation interval.

The spatial model of phase diagram greatly expands the possibilities of computer-aided design of materials. In particular, a solution for the problem of type changing of three-phase reaction was obtained, which cannot be realised either by thermodynamic calculations or by calculations from first principles.

Keywords: Phase diagram, Computer simulation, Cu-Ni-Mn system, Change of three-phase reaction type, Crystallisation interval, Microstructure

Funding: This work was been performed under the program of fundamental research IPMS SB RAS, project No. 0270-2021-0002.

For citation: Zelenaya A. E., Lutsyk V. I., Baldanov V. D. Computer model of Cu–Ni–Mn isobaric phase diagram: verification of crystallisation intervals and change of three-phase reaction type. *Condensed Matter and Interphases*. 2022;24(4): 466–474. https://doi.org/10.17308/kcmf.2022.24/10551

Для цитирования: Зеленая А. Э., Луцык В. И., Балданов В. Д. Компьютерная модель изобарной фазовой диаграммы Cu–Ni–Mn: верификация интервалов кристаллизации и смены типа трехфазной реакции. *Конденсированные среды и межфазные границы*. 2022;24(4): 466–474. https://doi.org/10.17308/kcmf.2022.24/10551

✉ Anna E. Zelenaya, e-mail: zel_ann@mail.ru

1. Introduction

Information about phase equilibria in the Cu–Mn–Ni system is of great importance for the creation of high-quality materials and solders with high physical and mechanical properties and corrosion resistance. In studies [1–2], the effect of addition of copper, nickel, and manganese for the creation of shape-memory alloys, as well as improvement of the physical properties of such alloys with the addition of manganese was studied. The study [3] investigated the thermoelectric properties of alloys based on the Cu–Ni–Mn system.

The high-temperature part of the phase diagrams of binary systems Cu–Mn, Mn–Ni and Cu–Ni is well studied. According to the generalised experimental data [4–5], a minimum is formed on the liquidus and solidus lines at 871 °C and 33.7 wt. % Mn in the Cu–Mn system. The system is also characterised by the occurrence of a metatectic reaction involving two high-temperature polymorphic modifications of manganese δMn and γMn at 1099 °C: δMn → L + γMn. In [6–7], a detailed study in the high-temperature part of the diagram rich in manganese, aimed at establishing the boundaries of phase regions with δMn and γMn was performed. Phase diagrams obtained using thermodynamic calculation methods [8–14] are in good agreement with experimental data.

The Mn–Ni system has a similar structure in the high-temperature part and also contains a minimum point on the liquidus and solidus lines at 1020 °C and 58.4 wt. % Mn, but unlike the Cu–Mn system, the transition from the polymorphic form δMn to form γMn occurs according to the peritectic scheme at 1170 °C: L + δMn → γMn [6, 15–16]. The data of the experimental study were confirmed by the results of thermodynamic calculations [8, 17–18]. The Cu–Ni system has the simplest topological structure and is characterised by the formation of continuous range of the solid solutions without extrema on the liquidus and solidus lines [4–5, 8, 19–21].

For the Cu–Mn–Ni ternary system, in the earliest studies [22–25], isotherms were obtained for the liquidus and solidus surfaces in the temperature range of 1440–800 °C and six isopleths. A simplified version of the diagram with the formation of continuous range of the solid solutions between all components and with the absence of a univariant line separating the fields of the onset of continuous crystallisation of solid solutions based on various polymorphic modifications of manganese was shown. At the same time, it was stated that if a line connecting the minimum points in the Cu–Mn and Mn–Ni binary systems is drawn, then the liquidus and solidus surfaces will adjoin along this line [24].

This assumption was also analysed graphically based on hypothetical phase diagrams with unlimited solubility of components and ternary points of minimum and maximum and corresponding extrema in all binary systems [26]. It was shown that the systems have contact lines between the liquidus and solidus surfaces in the direction from binary extrema to the ternary one. Isothermal sections with contact of liquidus and solidus isotherms along these lines were shown. At the same time, at the point of contact of the liquidus and solidus isotherms, both two fragments of the two-phase region L + S and two single-phase regions (L and S) adjoin. Such sections are typical for the section of saddle surfaces [27–28]. In [28], when discussing a similar diagram with maxima, the author described the contact between surfaces only at binary maximum points and at a ternary maximum point. On the section, only binary maximum points correspond to the contact of the liquidus and solidus isotherms.

In [29], using the example of the Cu–Mn–Ni system, the contact of the liquidus and solidus surfaces along the line connecting the points of binary minima was proved using the Gibbs phase rule. Based on the example of an isothermal section of a two-phase region without taking into account the contact of surfaces, it was shown that, assuming two degrees of freedom, two pairs of phases are in equilibrium, which contradicts the Gibbs phase rule. If the liquidus and solidus isotherms have a point of contact with a zero crystallisation interval, then, according to the authors, the violation of the phase rule does not occur. According to the calculations [30], it was shown that this line of contact of the liquidus and solidus between two minimum points is not straight. Experimental confirmation of the line corresponding to alloys with a zero crystallisation interval in the concentration range (35–44%

Mn, 0–15% Ni) was carried out in [31]. However, in later studies [32-33] the statement about the existence of a line of contact between the liquidus and solidus surfaces on the Cu–Mn–Ni diagram was proven to be false. According to the DTA data using the regression analysis method, the equations of the liquidus and solidus surfaces for the region of the Cu–Ni–Mn phase diagram from 0 to 20% Ni and from 30 to 50% Mn were calculated, the isotherms of the surfaces and the values of the crystallisation interval for the selected section of the diagram were shown. In this case, the temperature difference between the liquidus and solidus surfaces increases as the distance from the Cu–Mn binary system to the centre of the diagram increases.

The surface of the beginning of primary crystallisation based on the Cu(Ni) solid solution and isopleth drawn from Cu through the middle of the Mn–Ni system was obtained using the methods of thermodynamic calculation [34]. The authors [25] already calculated both liquidus surfaces corresponding to Mn and Cu(Ni) and six isopleths for the high-temperature part of the diagram. The sections were arranged in pairs parallel to the binary sides. On two sections located parallel to the binary systems Mn–Ni (at 20% Cu) and Cu–Mn (at 20% Ni), contact of the section lines of the liquidus and solidus surfaces was recorded, on two other similar sections there was no contact between the lines. It should be noted that when discussing systems Cu–Ti–Zr [35] and Ti–$TiMn_2$–$ZrMn_2$–Zr [36], containing binary systems with a minimum, points of contact of the section lines at the boundary of the three-phase regions with the melt were revealed on the isopleths.

2. Computer model of the phase diagram of the Cu–Mn–Ni system, taking into account the zero crystallisation interval

A computer model of the high-temperature part of the phase diagram above 800 °C has been developed. When constructing a computer model of the Cu–Mn–Ni (A–B–C) system, the formation of two high-temperature polymorphic modifications of manganese (δMn = B, γMn = B1) and minimum points in Cu–Mn binary systems (min_{AB}) and Mn–Ni (min_{BC}) was taken into account. We used data on the structure of binary systems according to the reference book [5] (Table 1) and the assumption that the liquidus and solidus surfaces come into contact along the line connecting the binary minima [22–24, 26, 29–31]. Invariant ternary points with the involvement of the melt in the system were not present in the system; therefore, the scheme of phase reactions has a simplified form (Scheme 1).

The model was developed based on the methodology of assembling it from phase regions and surfaces using the author's software products [37–38].

The high-temperature part of the phase diagram of the Cu–Mn–Ni system above 800 °C was formed by three pairs of liquidus, solidus, and transus surfaces (upper «liquidus» surface t^q_{B1} and lower «solidus» surface t^s_{B1}), and three ruled surfaces with a horizontal arrangement of the generating segment (Table 2). It includes two

Scheme 1. Scheme of phase reactions involving high-temperature manganese allotropes

Cu–Mn (A–B)	Cu–Mn–Ni (A–B–C)	Cu–Ni (A–C)	Mn–Ni (B–C)
$B \rightarrow L+B1$ (1170 °C) $k_{AB}k_{BC}$, $B^{B1}{}_{A}B^{B1}{}_{C}$, $B1^{B}{}_{A}B1^{B}{}_{C}$	→		$L+B \rightarrow B1$ (1099 °C) $k_{AB}k_{BC}$, $B^{B1}{}_{A}B^{B1}{}_{C}$, $B1^{B}{}_{A}B1^{B}{}_{C}$

Table 1. Coordinates of points on the contour of surfaces (z_i – weight fractions of components A, B, and C)

	z_1	z_2	z_3	T		z_1	z_2	z_3	T
A = Cu	1	0	0	1084.87	k_{AB}	0.27	0.73	0	1099
B = Mn	0	1	0	1246	B^{B1}_{A}	0.142	0.858	0	1099
C = Ni	0	0	1	1455	$B1^{B}_{A}$	0.132	0.868	0	1099
B1	0	1	0	1143	k_{BC}	0	0.902	0.098	1170
min_{AB}	0.663	0.337	0	871	B^{B1}_{C}	0	0.963	0.037	1170
min_{BC}	0	0.584	0.416	1020	$B1^{B}_{C}$	0	0.942	0.058	1170

Table 2. Surface contours

Symbol	Contour	Символ	Symbol
Liquidus			
q_B	Mn–k_{AB}–k_{BC}	q_{AC}	Cu–min_{AB}–k_{AB}–k_{BC}–min_{BC}–Ni
Solidus			
s_B	Mn–B_C^{B1}-B_A^{B1}	s_{AC}	Cu-min_{AB}–$B1_A^B$–$B1_C^B$–min_{BC}–Ni
Transus			
t_{B1}^q	B1–B_C^{B1}–B_A^{B1}	t_{B1}^s	B1–$B1_A^B$–$B1_C^B$
Ruled surfaces			
q_{AB}^r	k_{AB}–k_{BC}–$B1_C^B$–$B1_A^B$	s^r	$B1_A^B$–$B1_C^B$-B_C^{B1}-B_A^{B1}
q_{BA}^r	k_{AB}–k_{BC}–B_C^{B1}–B_A		

Table 3. The structure of the phase regions

Phase regions	Surfaces	Phase regions	Surfaces
L + B(TP)	q_B, s_B, q_{BA}^r	B	t_B^q, t_B^s
L + B1(TP)	q_{AC}, s_{AC}, q_{AB}^r	B1	s_{AC}, t_B^s
L + B + B1	q_{AB}^r, q_{BA}^r, s^r	B + B1	t_B^q, t_B^s, s^r

one-phase (B, B1), three two-phase (L + B (SS), L + B1 (SS), B + B1) and one three-phase (L + B + B1) regions (Table 3) (SS – solid solution). Designations B and B1 correspond to two forms of high-temperature manganese allotropy. Since the points on the horizontal segments corresponding to the metatectic and peritectic reactions are located very close, the prototype of the phase diagram was initially developed, in which the points were separated by compositions and temperatures while maintaining the topological structure (Fig. 1a–b). Such a prototype provides the possibility of more visual representation of the phase diagram, understanding the structure of the phase regions and interpretation of the sections. When introducing the coordinates of real points into the prototype [5] (Table 1), the final model of the phase diagram of the Cu–Mn–Ni system (Fig. 1c–d) is obtained.

3. Results and discussion

3.1. Change of three-phase reaction type

Based on a computer model in the three-phase region L+B+B1, a change of the peritectic transformation (L + B → B1) to metatectic (B → L + B1) was revealed. The three-phase region L + B + B1 is bounded by three ruled surfaces q_{AB}^r, q_{BA}^r and s^r (Fig. 2a, c), while in the projection there is a crossing of their directing curves $B_A^{B1}B_C^{B1}$ and $B1_A^BB1_C^B$. The surface of the two-phase reaction abc, on which a change of three-phase reaction type occurs, is a ruled surface and it is determined using the algorithm for calculating the change of the mass increment sign of the phase L [39–40]. Three-phase region L + B + B1 with a surface of change of the three-phase reaction type abc for the phase diagram prototype (Fig. 2a–b) and the real Cu–Mn–Ni system (Fig. 2c–d) is shown in Fig. 2. This surface divides the L + B + B1 phase region into two parts, in its "upper" part, the peritectic reaction L + B → B1 occurs, in the "bottom" part metatectic reaction B → L + B1 takes place (Fig. 2b, d). This process is clearly demonstrated by the diagrams of vertical mass balance (Fig. 2e–f). For the prototype, the mass centre is designated as G_1, for a real system it is designated as G_2. For both mass centres in the three-phase region L + B + B1, the B1 phase portion first increases and the L and B phase portions decrease, which corresponds to the peritectic reaction L + B → B1. At 501.6 °C (Fig. 2e) and 1130.71 °C (Fig. 2f), the change of mass increment sign of the L phase occurs, i.e., the decrease in the L phase portion stops and its growth begins, which already corresponds to the metatectic reaction B → L+B1.

Concentration projection of the three-phase region L + B + B1, including the surface of the change of the three-phase reaction type abc, is divided into six fields, four of which differ in ongoing phase transformations and microstructure elements (Fig. 3, Table. 4). Fields 2, 3, and 6 are characterised by the

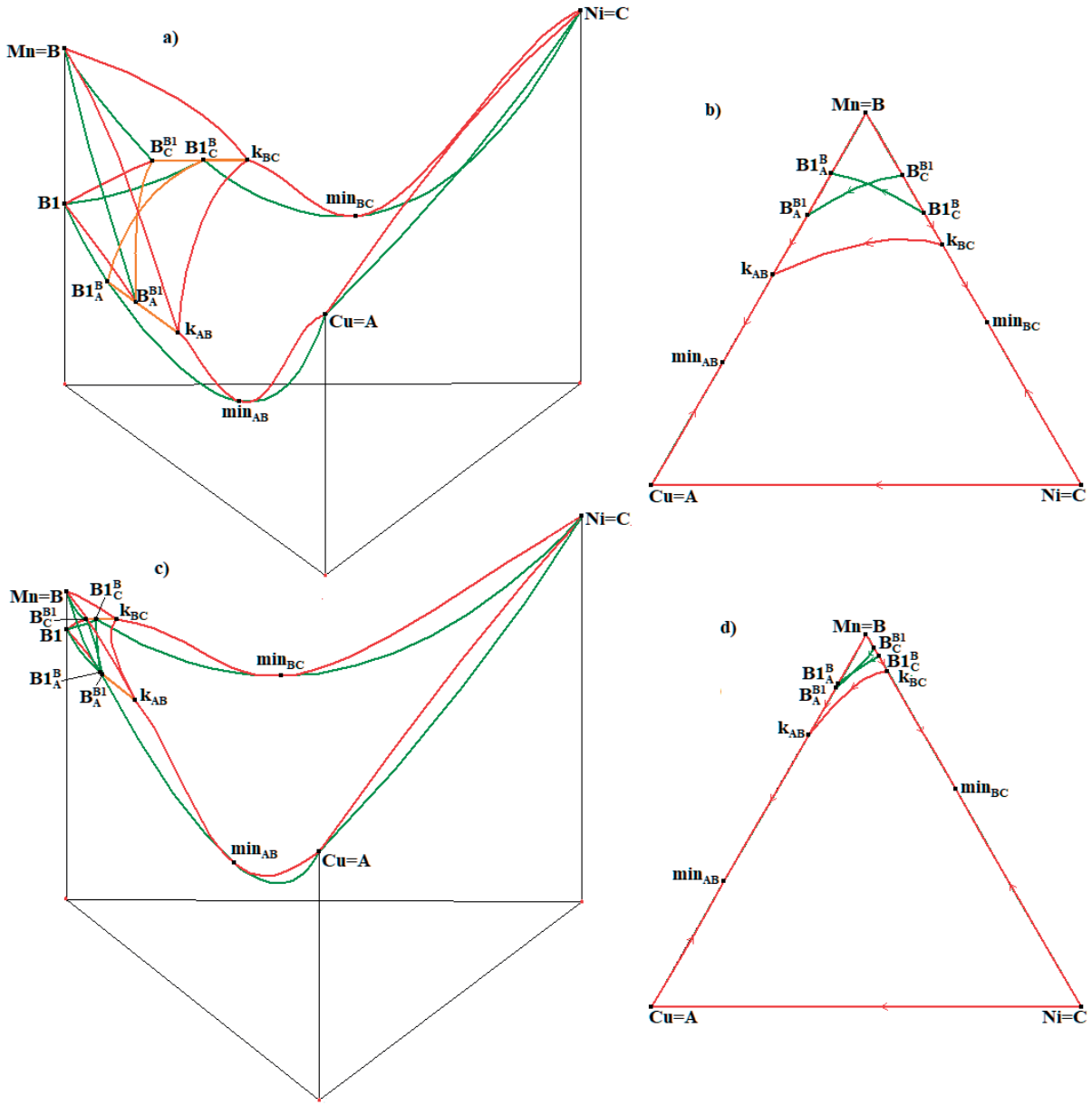

Fig. 1. 3D model and XY projection of the prototype (a–b) and the real Cu–Mn–Ni diagram (c–d)

Table 4 Microstructure formed in the three-phase region L + B + B1*

Field	Phase regions	Scheme of phase reactions	Microstructure
1	L + B(TP) B B + B1 L + B + B1	$L^1 \rightarrow B^1$, $B^1 \rightarrow B1^{1p}$, $B^m \rightarrow L^m + B1^m$	B^1, $B1^{1p}$, $B1^m$
2, 3, 6	L + B(TP) L + B + B1	$L^1 \rightarrow B^1$, $L^p + B \rightarrow B1^p$	B^1, $B1^p$
4	L + B(TP) L + B + B1	$L^1 \rightarrow B^1$, $B^m \rightarrow L^m + B1^m$	B^1, $B1^m$
5	L + B(TP) L + B + B1	$L^1 \rightarrow B^1$, $L^p + B \rightarrow B1^p$ $B^m \rightarrow L^m + B1^m$	B^1, $B1^p$, $B1^m$

* ^{1} – primary crystallisation, ^{1p} – primary postperitectic crystallisation, ^{p} – peritectic reaction, ^{m} – metatectic reaction

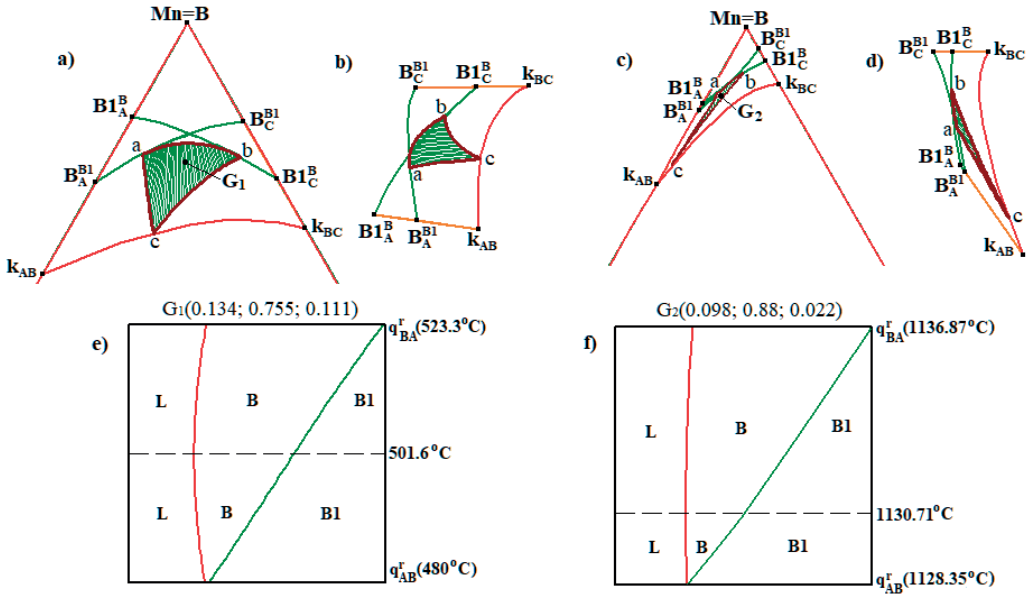

Fig. 2. XY projection and 3D model of the change surface of three-phase transformation type in the phase region L + B + B1 for the prototype (a–b) and the real system (c–d); calculation of the diagrams of vertical mass balances for mass centres G1(e) and G2(f)

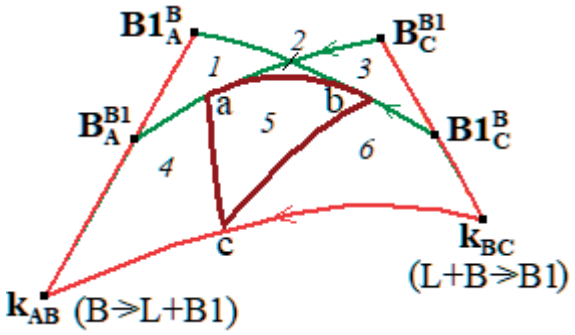

Fig. 3. Projection of three-phase region L + B + B1 with division into concentration fields

formation of primary crystals B^1 and crystals $B1^p$, resulting from the peritectic reaction. Fields 1 and 4 contain primary crystals B^1 and crystals $B1^m$ released as a result of a metatectic reaction. However, since these two fields differ in crystallisation stages, field 1 additionally includes primary crystals $B1^{1p}$. Field 5 besides B^1, includes microstructures such as $B1^p$, and $B1^m$, since it is the surface on which the change of the three-phase reaction type takes place.

3.2. Calculation of isothermal sections

Calculation of isothermal sections based on the prototype in the temperature range between two minimum points min_{AB} and min_{BC} is shown in Fig. 4. On the section coinciding with the temperature of the minimum point min_{BC} (Fig. 4a), the liquidus and solidus isotherms adjoin at this point. As the temperature decreases, the liquidus and solidus isotherms gradually approach the minimum min_{AB}. Since the model was constructed taking into account the zero crystallisation interval, there is contact between isotherms along the $min_{AB}min_{BC}$ line (Fig. 4b–e). The point of contact of the liquidus and solidus isotherms is a common boundary between the one-phase regions L and B1 and two fragments of the two-phase region L + B1(SS). At minimum temperature min_{AB} the isotherms merge into a point, and only one phase B1 remains in the section.

Since the question of the crystallisation interval along the line connecting the minimum points remains controversial, an additional model of the phase diagram of the Cu–Mn–Ni system was developed with a non-zero value of the crystallisation interval along the $min_{AB}min_{BC}$ line. An isothermal section for such a variant of the diagram is shown in Fig. 4e. In this case, the one-phase regions corresponding to the melt L and the solid phase B1 are separated by a two-phase region L+B1(SS).

4. Conclusions

A computer model of the phase diagram of the Cu–Mn–Ni system above 800 °C has been developed. The high-temperature part of

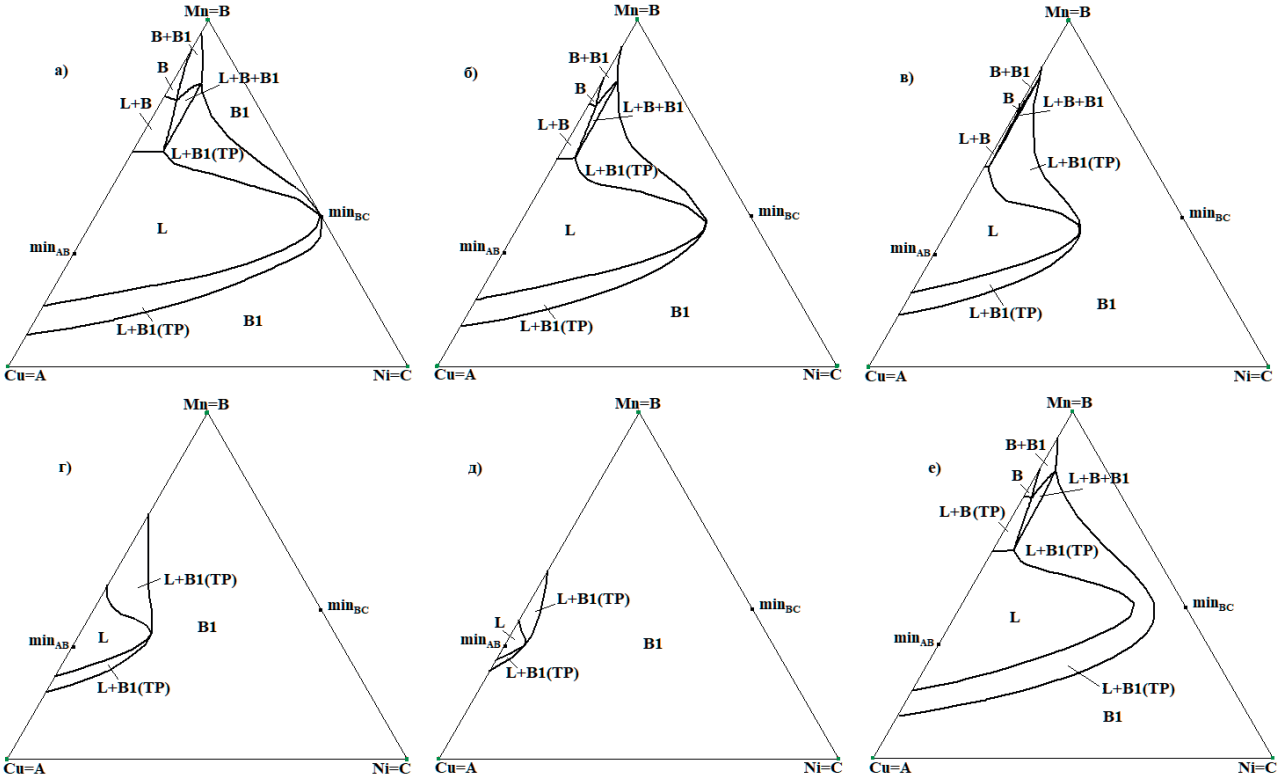

Fig. 4. Isothermal sections for the phase diagram prototype with zero crystallisation interval along the line $min_{AB}min_{BC}$ at T_{minBC} = 450 °C (a), 414 °C (b), 376 °C (c), 338 °C (d), 310 °C (e); isothermal section at 414 °C in the presence of crystallisation interval (f)

the diagram includes 9 surfaces and 6 phase regions. It was revealed that in the three-phase region L+B+B1 there is a change from peritectic equilibrium to monotectic equilibrium, which was confirmed by the calculation of material balance diagrams. Three-phase region, taking into account the surface of type change of three-phase reaction, is divided into six concentration fields when projecting into the composition triangle. Four concentration fields differ in the crystallisation stages and the formed set of microstructures. Based on the prototype of the phase diagram, the calculation of isothermal sections in the temperature range between two minimum points in the Cu–Mn and Mn–Ni binary systems was carried out. Taking into account the crystallisation interval in the sections, the two-phase region L + B1(SS) separates the one-phase regions L and B1. At a zero crystallisation interval along the line connecting the minimum points, a point of contact of the liquidus and solidus isotherms appears on the sections. At this point, the one-phase regions L and B1 and two parts of the two-phase region L + B1 (SS) are in contact.

The spatial computer model allowed us to obtain a solution to the problem, which cannot be achieved using thermodynamic calculations and calculations based on first principles. The presented methodology can also be applied to other systems with Mn, where the effect of a change of the type of phase reaction in the three-phase region with two high-temperature modifications of Mn can be revealed [41-44].

Author contributions

All authors made an equivalent contribution to the preparation of the publication.

Conflict of interests

The authors declare that they have no known competing financial interests or personal relationships that could have influenced the work reported in this paper.

References

1. Akash K., Mani Prabu S. S., Gustmann T., Jayachandran S., Pauly S., Palani I. A. Enhancing the life cycle behaviour of Cu–Al-Ni shape memory alloy bimorph by Mn addition. *Materials Letters*. 2018;226: 55–58. https://doi.org/10.1016/j.matlet.2018.05.008

2. Gera D., Santos J., Kiminami C. S., Gargarella P. Comparison of Cu–Al–Ni–Mn–Zr shape memory alloy prepared by selective laser melting and conventional powder metallurgy. *Transactions of Nonferrous Metals Society of China*. 2020;30(12): 3322–3332. https://doi.org/10.1016/S1003-6326(20)65464-4

3. Kang H., Yang Z., Yang X., Li J., He W., Chen Z., Guo E., Zhao L.-D., Wang T. Preparing bulk Cu–Ni-Mn based thermoelectric alloys and synergistically improving their thermoelectric and mechanical properties using nanotwins and nanoprecipitates. *Materials Today Physics*. 2021;17: 100332. https://doi.org/10.1016/j.mtphys.2020.100332

4. *Binary alloy phase diagrams*. Vol. 1. Massalski T. B. (ed.). Ohio: American Society for Metals, Metals Park; 1986. 1100 p.

5. *State diagrams of binary metal systems**. Vol. 2. Ljakishev N. P. (ed.). Moscow: Mashinostroenie Publ.; 1997. 1024 p. (In Russ.)

6. Hellawell A., Hume-Rothery W. The construction of alloys of iron and manganese with transition elements of the first long period. *Philosophical Transactions of the Royal Society of London. Series A, Mathematical and Physical Sciences*. 1957;249: 417–459. http://doi.org/10.1098/rsta.1957.0004

7. Wachtel E., Terzieff P., Bahle J. Aufbau und magnetische Eigenschaften manganreicher Cu–Mn– und Mn–Sn-Legierungen. *Monatshefte für Chemie*. 1986;117(12): 1349–1366. http://doi.org/10.1007/bf00810745

8. Kaufman L. Coupled phase diagrams and thermochemical data for transition metal binary systems-VI. *Calphad*. 1979;3(1): 45–76. https://doi.org/10.1016/0364-5916(79)90020-8

9. Lewin K., Sichen D., Seetharaman S. Thermodynamic study of the Cu–Mn system. *Scandinavian Journal of Metallurgy*. 1993;22(6): 310–316. Available at: https://www.researchgate.net/publication/262068679_Thermodynamic_study_of_the_Cu–Mn_system

10. Miettinen J. Thermodynamic description of the Cu–Mn–Zn system in the copper-rich corner. *Calphad*. 2004;28(3): 313–320. https://doi.org/10.1016/j.calphad.2004.09.003

11. Turchanin M. A., Agraval P. G., Abdulov A. R. Phase equilibria and thermodynamics of binary copper systems with 3d-metals. IV. Copper – Manganese system. *Powder Metallurgy and Metal Ceramics*. 2006;45(11–12): 569–581. https://doi.org/10.1007/s11106-006-0121-y

12. Wang C. P., Liu X. J., Ohnuma I., Kainuma R., Ishida K. Thermodynamic assessments of the Cu–Mn–X (X: Fe, Co) systems. *Journal of Alloys and Compounds*. 2007;438(1–2): 129–141. https://doi.org/10.1016/j.jallcom.2006.08.018

13. He C., Du Y., Chen H.-L., Liu S., Xu H., Ouyang Y., Liu Z.-K. Thermodynamic modeling of the Cu–Mn system supported by key experiments. *Journal of Alloys and Compounds*. 2008;457(1–2): 233–238. https://doi.org/10.1016/j.jallcom.2007.03.041

14. Cui S., Jung I.-H. Thermodynamic modeling of the Cu–Fe–Cr and Cu–Fe–Mn systems. *Calphad*. 2017;56: 241–259. https://doi.org/10.1016/j.calphad.2017.01.004

15. *Binary alloy phase diagrams*. Vol. 2. Massalski T. B. (ed.). Ohio: American Society for Metals, Metals Park; 1986. 2224 p.

16. Gokcen N. A. The Mn–Ni (manganese-nickel) system. *Journal of Phase Equilibria*. 1991;12(3): 313–321. https://doi.org/10.1007/BF02649919

17. Miettinen J. Thermodynamic solution phase data for binary Mn–based systems. *Calphad*. 2001;25(1): 43–58. https://doi.org/10.1016/S0364-5916(01)00029-3

18. Guo C., Du Z. Thermodynamic optimization of the Mn–Ni system. *Intermetallics*. 2005;13(5): 525–534. https://doi.org/10.1016/j.intermet.2004.09.002

19. an Mey S. Thermodynamic re-evaluation of the Cu–Ni system. *Calphad*. 1992;16(3): 255–260. https://doi.org/10.1016/0364-5916(92)90022-P

20. Turchanin M. A., Agraval P. G., Abdulov A. R. Phase equilibria and thermodynamics of binary copper systems with 3d-metals. VI. Copper-nickel system. *Powder Metallurgy and Metal Ceramics*. 2007;46: 467–477. https://doi.org/10.1007/s11106-007-0073-x

21. Tesfaye F., Vaajamo I., Hamuyuni J., Lindberg D., Taskinen P., Hupa L. Experimental investigation and thermodynamic re-assessment of the ternary copper-nickel-lead system. *Calphad*. 2018;61: 148–156. https://doi.org/10.1016/j.calphad.2018.03.006

22. Parravano N. Alloys of nickel, manganess, and copper. *Gazzetta Chimica Italiana*. 1913;42: 385–394.

23. Parravano N. Ternary alloys of iron-nickel-manganese, nickel-manganese-copper, and iron-manganese-copper. *Intern. Z. Metallog.* 1913;4: 171–202.

24. Anosov V. Ja., Pogodin S. A. *Fundamentals of physical and chemical analysis*. Moscow: Nauka Publ.; 1976. 504 p. (In Russ.)

25. Sun W., Xu H., Du Y., Liu S., Chen H., Zhang L., Huang B.-Y. Experimental investigation and thermodynamic modeling of the Cu–Mn–Ni system. *Calphad*. 2009;33(4): 642–649. https://doi.org/10.1016/j.calphad.2009.07.003

26. Pikunov M. V., Sidorov E. V. Phase diagrams of three-component systems corresponding to unbounded solid solutions with a temperature extremum. *Steel in Translation*. 2008;38(1): 1–4. https://doi.org/10.3103/S0967091208010014

27. Palatnik L. S., Landau A. I. *Phase Equilibria in Multicomponent Phase Diagrams*. New York: Holt Rinehart and Winston, Inc.; 1964. 454 p.

28. Petrov D. A. *Binary and ternary systems*. Moscow: Metallurgija Publ.; 1986. 256 p. (In Russ.)

29. Pikunov M. V., Sidorov E. V. Structure of the phase diagram of the Cu–Ni–Mn system. *Steel in*

Translation. 2008;38(5): 351–354. https://doi.org/10.3103/S096709120805001X

30. Bazhenov V. E., Pikunov M. V. Temperature-minimum line in the Cu–Ni–Mn phase diagram. *Steel in Translation*. 2010;40(3): 225–228. https://doi.org/10.3103/S0967091210030071

31. Pashkov A. I. *Research and development of technology for obtaining alloys of the Cu–Mn–Ni system by mechanical alloying for high-temperature soldering**. Cand. tech. sci. diss. Abstr. Moscow: 2009. 28 p. (In Russ.). Available at: https://www.dissercat.com/content/issledovanie-i-razrabotka-tekhnologii-polucheniya-splavov-sistemy-Cu-Mn–ni-metodom-mekhanich

32. Bazhenov V. E. *The study of crystallization processes of ternary alloys in order to assess their tendency to non-equilibrium crystallization**. Cand. tech. sci. diss. Abstr. Moscow: 2013. 25 p. (In Russ.). Available at: https://www.dissercat.com/content/izuchenie-kristallizatsionnykh-protsessov-troinykh-splavov-s-tselyu-otsenki-ikh-sklonnosti-k

33. Bazhenov E. V. On the Cu–Ni–Mn system state diagram. *Izvestiya Vuzov. Tsvetnaya Metallurgiya = Izvestiya. Non-Ferrous Metallurgy*. 2013;(1): 49–55. (In Russ., abstract in Eng.). https://doi.org/10.17073/0021-3438-2013-1-49-55

34. Miettinen J. Thermodynamic description of the Cu–Mn–Ni system at the Cu–Ni side. *Calphad*. 2003;27(2): 147–152. https://doi.org/10.1016/j.calphad.2003.08.003

35. Turchanin M. A., Velikanova T. Y., Agraval P. G., Abdulov A. R., Dreval' L. A. Thermodynamic assessment of the Cu–Ti–Zr system. III. Cu–Ti–Zr system. *Powder Metallurgy* and *Metal Ceramics*. 2008;47: 586–606. https://doi.org/10.1007/s11106-008-9062-y

36. Ivanchenko V. G., Pryadko T. V., Gavrylenko I. S., Pogorelaya V. V. Phase equilibria in the Ti–$TiMn_2$–$ZrMn_2$–Zr partial system. *Chemistry of Metals and Alloys*. 2008;1: 67–72. https://doi.org/10.30970/cma1.0004

37. Lutsyk V. I., Zelenaya A. E., Zyryanov A. M. Multicomponent systems simulation by the software of "Diagrams Designer". *Journal of International Scientific Publications: Materials, Methods & Technologies*. 2008;2: 176–184. Available at: https://www.scientific-publications.net/download/materials-methods-and-technologies-2008.pdf

38. Vorob'eva V. P., Zelenaya A. E., Lutsyk V. I., Lamueva M. V. A 3D computer model of the CaO–MgO–Al_2O_3 *T-x-y* diagram at temperatures above 1300 °C. *Condensed Matter and Interphases*. 2021;23(3): 380–386. https://doi.org/10.17308/kcmf.2021.23/3529

39. Lutsyk V. I., Vorob'eva V. P. Investigation of the conditions for changing the type of three-phase transformation in the Ti–Ir–Ru system. *Perspektivnye materialy = Perspective materials*. 2011;(S13): 191–198. (In Russ., abstract in Eng.). Available at: https://elibrary.ru/item.asp?id=17635587

40. Lutsyk V. I., Zelenaya A. E., Zyryanov A. M. Specific features of the crystallization of melts in systems with a transition from syntectic equilibrium to monotectic equilibrium. *Crystallography Reports*. 2009;54(7): 1300–1307. https://doi.org/10.1134/S1063774509070281

41. Kainzbauer P., Richter K. W., Effenberger H. S., Giester G., Ipseret H. The ternary Bi-Mn–Sb phase diagram and the crystal structure of the ternary* phase $Bi_{0.8}MnSb_{0.2}$. *Journal of Phase Equilibria and Diffusion*. 2019;40: 462–481. https://doi.org/10.1007/s11669-019-00719-x

42. Florian G., Gabor A. R., Nicolae C. A. … Rotaru P. Thermomechanical, calorimetric and magnetic properties of a Ni–Ti shape-memory alloy wire. *Journal of Thermal Analysis and Calorimetry*. 2020;140(2): 147–527. https://doi.org/10.1007/s10973-019-08869-3

43. Li H., Ruan J., Ueshima N., Oikawa K. Experimental investigations of fcc/bcc phase equilibria in the Cr–Mn–Ni ternary system. *Intermetallics*. 2020;127: 106994. https://doi.org/10.1016/j.intermet.2020.106994

44. Ruan J., Ueshima N., Li H., Oikawa K. Phase equilibria, martensitic transformations and deformation behaviors of the subsystem of Cantor alloy-low-cost Fe–Mn–Cr alloys. *Materialia*. 2021;20: 101231. https://doi.org/10.1016/j.mtla.2021.101231

* *Translated by author of the article.*

Information about the authors

Anna E. Zelenaya, Cand. Sci. (Phys.–Math.), Senior Researcher of the Sector of Computer Materials Design, Institute of Physical Materials Science, Siberian Branch of the Russian Academy of Sciences (Ulan-Ude, Russian Federation).

https://orcid.org/0000-0001-5232-8567

zel_ann@mail.ru

Vasily I. Lutsyk, Dr. Sci. (Chem.), Head of the Sector of Computer Materials Design, Institute of Physical Materials Science, Siberian Branch of the Russian Academy of Sciences (Ulan-Ude, Russian Federation).

https://orcid.org/0000-0002-6175-0329

vluts@ipms.bscnet.ru

Viktor D. Baldanov, post-graduate student of the Sector of Computer Materials Design, Institute of Physical Materials Science, Siberian Branch of the Russian Academy of Sciences (Ulan-Ude, Russian Federation).

https://orcid.org/0000-0002-3946-9565

victor_baldanov@mail.ru

Received 08.06.2022; approved after reviewing 12.07.2022; accepted for publication 15.09.2022; published online 25.12.2022.

Translated by Valentina Mittova

Edited and proofread by Simon Cox